Check for
updates

On the Coupled Transient Hygrothermal Analysis in the Porous Cylindrical Panels

Yaghoub Tadi Beni[1] · **Jaber Alihemmati**[2]

© The Author(s), under exclusive licence to Springer Nature B.V. 2021

Abstract

In this paper, transient coupled heat and moisture transfer in the cylinders and cylindrical panels of the porous medium are analyzed with three-dimensional finite element methods. Both Dofour and Soret effects are considered in the formulation, and the FEM-based weak forms of the equations are derived using Galerkin method. In the full cylinder cases, both symmetrical and unsymmetrical boundary conditions for heat and moisture are applied to cover three-dimensional and axisymmetric (two dimensional) analysis cases. The obtained systems of time-dependent differential equations are solved by Runge–Kutta method. The main objective of the present study is the analysis of fully coupled diffusion of heat and moisture in cylindrical coordinates using three-dimensional finite element methods. Also, this study addressed the ability of Runge–Kutta method to solve the coupled sets of differential equations. The results were compared with some analytical solutions in the literature, and a very good agreement was observed. The present formulation can be used for transient analysis of any cylindrical geometry with arbitrary geometrical dimensions and under desired boundary conditions.

Keywords Three-dimensional finite element · Coupled heat and moisture transfer · Porous materials · Cylindrical panels

1 Introduction

The diffusion of heat in a solid is recognized by the Fourier law. This law states that the heat in a solid is transferred from higher to lower temperature locations, and the heat flux in a certain direction is proportional to the temperature gradient on those directions (Incropera et al. 2006). The moisture diffusion is a physical phenomenon that basically happen in the same manner as heat diffusion, the moisture is transferred from higher moisture concentration to lower concentration locations, and the moisture flux is proportional to the gradient of moisture concentration; this is recognized as Fick law (Fick 1855).

✉ Yaghoub Tadi Beni
   tadi@sku.ac.ir

1   Faculty of Engineering, Shahrekord University, Shahrekord, Iran

2   Mechanical Engineering Department, Shahrekord University, Shahrekord, Iran

⧜ Springer

The dependence of temperature and moisture diffusion is introduced by Soret and Dufour effects. The Soret effect is the induction of moisture flow due to non-uniform temperature distribution in a solid with uniform moisture distribution, and the Soret effect is related to the creation of heat flow due to non-uniform moisture distribution in a solid with uniform temperature distribution (Sih et al. 1986).

One of the major problems in the coupled theory of heat and moisture diffusion is that the coupling coefficients are not known experimentally (Sih et al. 1986). By some assumptions, these coefficients can be determined analytically. By knowing the temperature and moisture diffusivity that can be determined by experiment, the numerical values of coupling constants can be derived by comparison of the transient moisture distributions between coupled and uncoupled solutions for the problems of weak coupling between heat and moisture (Sih et al. 1986). It can be the major reason that one cannot find a considerable number of research studies which deal with the analysis of coupled diffusion of heat and moisture; nevertheless, several studies have been conducted in this field a brief review of which is as follow:

Chang and Weng (2000) proposed an analytical solution for coupled heat and moisture transfer in porous materials. They subjected the equations to Laplace transform to reduce them into ordinary differential equations, and then, they solved the ordinary differential equations by introducing a transformation method.

Zhang et al. (2015) performed a solution for coupled heat and moisture transfer in building material. They solved the coupled differential equations using Laplace transform for a one-dimensional wooden media and obtained close form equations for temperature and moisture distributions.

Chang (1994) proposed an analytical solution for the transient hygrothermal response of infinitely long symmetric solid cylinders. He first decoupled the differential equations using some algebraic techniques and then solved the decoupled equations using separation of variables. He obtained the temperature and moisture distribution in terms of radial special coordinate and time. He concluded that the influence of coupling between temperature and moisture is significant for T300/5208 composites.

Simulation of heat and moisture transfer in a typical earth-sheltered building envelope was carried out by Ma et al. (2009). They simulate a two-dimensional section of building in FEM-based software (COMSOL multiphysics). They concluded that the coupling between heat and moisture should be considered where the investigation of heat transfer in porous materials is of interest. As in three-dimensional research examples, Cinefra et al. (2017a, b) studied the hygrothermal analysis of multilayered composite plates by variable kinematics finite elements. Also in another work, Cinefra et al. (2017a, b) used the variable kinematics shell elements for composite laminates accounting for hygrothermal effects. In both studies, they considered one- and three-dimensional temperature and moisture distributions and solved the Fourier heat conduction and Fick law equations by an analytical method. It should be mentioned that any coupling effects between temperature and moisture are not taken into account in these works, and heat and moisture equations are solved independently.

Also, there are more studies dealing with the analysis of porous structures in the literature that are mentioned in the next.

Malekzadeh Fard and Pourmoayed (2020) investigated the weight optimization of the prismatic core sandwich panel under transverse and longitudinal loadings, independently. They used a new improved constrained differential evolution (ICDE) algorithm to solve the optimization problems.

Kumar et al. (2020) used a refined beam theory to vibration analysis of single-walled carbon nanotube (SWCNT). The SWCNT exposed to both the hygroscopic as well as thermal environments, and the thermal environment was considered as a nonlinear thermal stress field based on Murnaghan's model, whereas the hygroscopic environment was assumed as a linear stress field. Saadatfar (2020) analyzed the problem of time-dependent stress redistribution of a piezomagnetic rotating thick-walled cylinder under an axisymmetric hygro-thermo-magneto-electro-mechanical loading. They concluded that creep analysis is vital for the materials that their properties are dependent to temperature and moisture since the effect of temperature and moisture dependency is more significant after creep progress rather than the initial case.

Dastjerdi et al. (2020a, b) investigated the size- and time-dependent viscoelastic bending analysis of rotating functionally graded nanostructures. They assumed that the structure rotates around two axes with constant angular accelerations as a gyroscopic. Dynamic instability of viscoelastic porous functionally graded (FG) nanobeam embedded on visco-Pasternak medium was investigated by Jalaei and Civalek (2019).

Fallahi et al. (2020) investigated the effect of the fiber orientation on the mechanical response of variable angle tow (VAT) panels. Effects of material properties, geometries, and boundary conditions on the static, free vibration, and buckling response of panels were performed. Reshad Noori et al. (2021) introduced an efficient numerical procedure to the solution of the dynamic response of functionally graded porous (FGP) beams. They assumed that the elastic modulus and mass density of the porous materials change through the thickness direction.

Yapor Genao et al. (2021) used a displacement-based nonlinear finite element model for functionally graded porous micro-plates. Different distributions of porosity with a constant volume of voids were employed in their work. Also, the power-law distribution was considered to model the variation of the two material constituents, while the porosity distributions vary according to cosine functions.

Bisheh and Civalek (2020) studied the vibration of smart laminated carbon nanotube-reinforced composite cylindrical panels on elastic foundations in hygrothermal environments. They used the Mori–Tanaka micromechanics model for estimating the effective material properties of the panel, and first-order shear deformation theory was used for extracting the governing equation.

The static deflection and free vibration problem of functionally graded porous cylindrical micro/nanoshells were analyzed by Salehipour et al. (2019). The modified couple stress theory was used for consideration of small-scale effects, and the governing equations of first-order shear deformation theory were employed and solved by generalized differential quadrature method. Arefi et al. (2020) studied the size-dependent deflection of FG graphene nanoplatelets (GNPs) reinforced composite micro-plates with porosity subjected to a transverse load. They used the various models for the distribution of porosity and GNPs in their analysis. Ghobadi et al. (2021) investigated the effect of the diverse distribution of porosity on the static and nonlinear dynamic responses of a sandwich functionally graded nanostructure with thermo-electro-elastic coupling based on the modified flexoelectric theory.

Dastjerdi et al. (2020a, b) used a highly efficient quasi-three-dimensional theory to study the nonlinear hygro-thermo-mechanical bending analysis of a very thick functionally graded material rotating disk in a hygro-thermal environment considering the porosity as a structural defect.

Salehipour et al. (2020) studied the bending and free vibration of porous and functionally graded cylindrical micro/nanoshells based on the modified couple stress and

three-dimensional elasticity theories. Dastjerdi and Beni (2019) presented the static analysis of macro- and nano-sector plates with variable thickness. The governing equations were derived based on the nonlocal modified higher-order shear deformation theory and were solved by applying the semi-analytical polynomial method.

Kim et al. (2019) investigated the bending, free vibration, and buckling response of functionally graded porous microplates. The Navier solution technique was utilized to obtain the analytical solutions for simply supported rectangular plates. Jankowski et al. (2020) studied the effects of porous material on bifurcation buckling and natural vibrations of nanobeams based on the higher-order nonlocal strain gradient theory. Dastjerdi et al. (2021) presented a novel quasi-three-dimensional approach for the bending analysis of moderately thick plates with a functionally graded material, in the presence of porosities.

Also, many researchers studied the thermodynamic and fluid flow in porous materials; some examples are as follows: Lv et al. (2021) studied the effect of gas adsorption on the effective stress of coal under triaxial stress experimentally. They considered the deformation due to the pore pressure and the swelling deformation of the coal matrix induced by adsorption separately, by injecting both sorptive and non-sorptive gases into a coal sample with different pore pressures. Straughan (2020) investigated the nonlinear stability in a model for thermal convection in a saturated porous material using Brinkman's theory. They used models for viscous dissipation by assuming that the flow in the porous medium may be described by a theory for a mixture of an elastic solid and a linearly viscous fluid.

As can be seen from the above-mentioned works, the fully coupled heat and moisture transfer phenomenon have been studied in some one- and two-dimensional cases and most of the studies have focused on the effects of temperature and moisture on the structural response of the solid structures. Therefore, a fully coupled three-dimensional analysis of heat and moisture transfer can give more detailed information of the phenomenon which need in real-world engineering designs. The main objective of the present work is a fully coupled three-dimensional analysis of heat and moisture transfer without any assumptions. Also, the present work employs the three-dimensional finite element method for solving the governing equations and represents the ability and accuracy of FEM for solving these types of coupled differential equations.

Further, in the present work, transient coupled heat and moisture transfer in the cylindrical panels constructed of porous materials are solved using three-dimensional finite element method. Also the results are compared with the same results in the literature and a good agreement will be observed. The proposed model can be used for the analysis of coupled and uncoupled heat and moisture transfer in any cylindrical body and can be developed to use for any 3D geometry. To show this ability, some case studies of three- and two-dimensional analysis of various cylindrical geometries are presented.

2 Problem Description and Governing Equations

A cylindrical panel constructed from a porous material referred to a cylindrical coordinate system and its geometrical parameters are shown in Fig. 1.

As illustrated in Fig. 1, r, θ, and z are the coordinates in radial, the circumferential, and axial direction of the cylindrical panel, respectively, and the panel has inner radius a, outer radius b, length L, and span angle α. All length dimensions (except for the comparison studies) in present work are in centimeters.
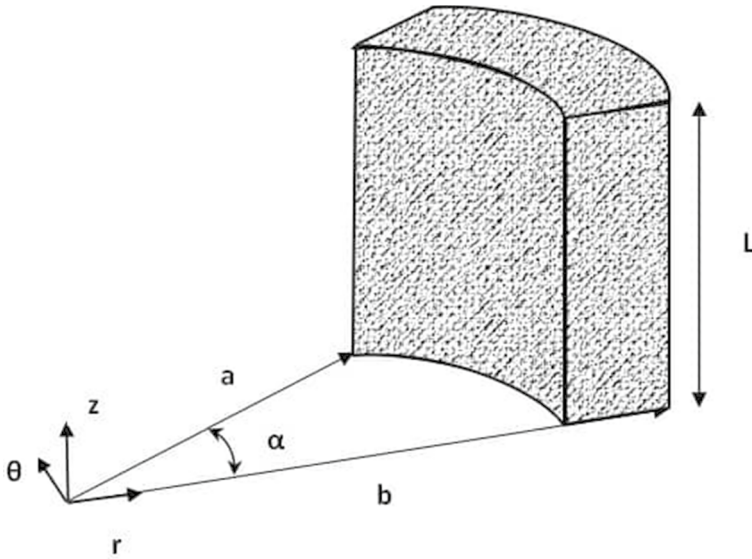
Fig. 1 Geometry and coordinate system of cylindrical panel

The coupled differential equations governing the temperature and moisture diffusions are as follow (Sih et al. 1986):

$$d_m \nabla^2 C + \lambda d_h \nabla^2 T = \frac{\partial C}{\partial t}$$
$$v d_m \nabla^2 C + d_h \nabla^2 T = \frac{\partial T}{\partial t}$$

(1)

where d_m and d_h are moisture and thermal diffusivity, v and λ are coupling coefficients, T and C represent the temperature and moisture concentration, respectively, and t denotes the time. The Laplace operator, ∇^2 in cylindrical coordinate, is as follow (Lai et al. 2010):

$$\nabla^2 = \frac{\partial^2}{\partial r^2} + \frac{1}{r}\frac{\partial}{\partial r} + \frac{1}{r^2}\frac{\partial^2}{\partial \theta^2} + \frac{\partial^2}{\partial z^2}$$

(2)

3 Finite Element Formulation

In FEM modeling, the first step is discretizing the problem domain into a set of elements and interpolate the field variables in such elements in terms of the unknown values attributed to the nods attached to elements (Segerlind 1984; Liu and Quek 2003). In this work, regarding to the problem coordinate system, we use the cylindrical element.

This element is a three-dimension element with a node in each corner of the element. Each node has two degrees of freedom, temperature and moisture concentration. For simplicity of coding and using numerical integration, the elements are mapped into a reference element in the reference coordinate system. Figure 2 shows the used cylindrical element and its mapping into the reference coordinate system. In the reference element, it can be
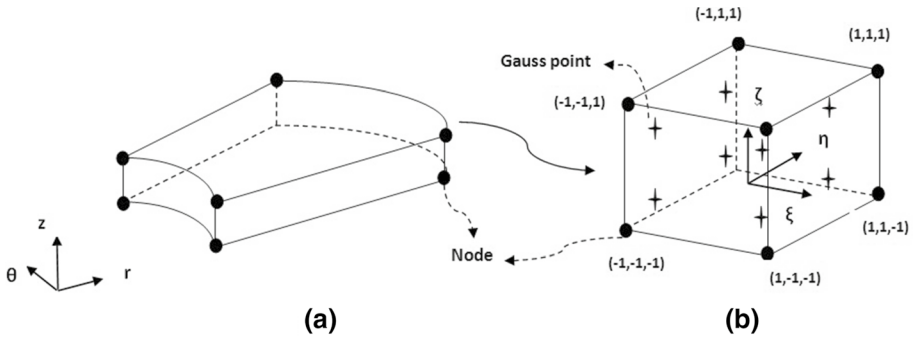
Fig. 2 Cylindrical element in physical (**a**) and reference (**b**) coordinate systems

seen that all dimensions of the element are mapped in the interval of $\begin{bmatrix} -1 & 1 \end{bmatrix}$. This is the standard mapping to use the Gauss integration and also to simplify the construction of element shape functions.

In this work, same elements are used for temperature and moisture approximation. Thus, in an arbitrary element, the temperature and moisture distributions are as follow (Segerlind 1984; Liu and Quek 2003):

$$
\hat{T} = \sum_{i=1}^{8} N_i T_i = N_1 T_1 + N_2 T_2 + \cdots N_8 T_8 = \mathbf{N}\overline{\mathbf{T}}
$$

$$
\hat{C} = \sum_{i=1}^{8} N_i C_i = N_1 C_1 + N_2 C_2 + \cdots N_8 C_8 = \mathbf{N}\overline{\mathbf{C}}
$$

(3)

In which $\hat{T}$ and $\hat{C}$ are temperature and moisture concentration in the element of interest and T_i and C_i are the unknown nodal value of temperature and moisture concentration, respectively, and $\overline{\mathbf{T}}$ and $\overline{\mathbf{C}}$ are vectors of local nodal value, N_i are element shape functions defined as follow (Segerlind 1984; Liu and Quek 2003):

$$
N_1 = \frac{1}{8}(1 - \xi)(1 - \eta)(1 - \gamma)
$$

$$
N_2 = \frac{1}{8}(1 + \xi)(1 - \eta)(1 - \gamma)
$$

$$
N_3 = \frac{1}{8}(1 + \xi)(1 + \eta)(1 - \gamma)
$$

$$
N_4 = \frac{1}{8}(1 - \xi)(1 + \eta)(1 - \gamma)
$$

$$
N_5 = \frac{1}{8}(1 - \xi)(1 - \eta)(1 + \gamma)
$$

$$
N_6 = \frac{1}{8}(1 + \xi)(1 - \eta)(1 + \gamma)
$$

$$
N_7 = \frac{1}{8}(1 + \xi)(1 + \eta)(1 + \gamma)
$$

$$
N_8 = \frac{1}{8}(1 - \xi)(1 + \eta)(1 + \gamma)
$$

(4)

And **N** is the matrix of shape functions defined as:

$$\mathbf{N} = \begin{bmatrix} N_1 & N_2 & \cdots & N_8 \end{bmatrix} \tag{5}$$

In the Galerkin finite element method, the shape functions themselves are used as weight functions to construct the residual (Segerlind 1984). By applying Galerkin method on Eq. (1), we have:

$$\iiint_{V^e} \mathbf{N^T} \left(\mathbf{D_m} \nabla^2 \overline{\mathbf{C}} + \lambda \mathbf{D_h} \nabla^2 \overline{\mathbf{T}} - \dot{\overline{\mathbf{C}}} \right) = 0$$

$$\iiint_{V^e} \mathbf{N^T} \left(\nu \mathbf{D_m} \nabla^2 \overline{\mathbf{C}} + \mathbf{D_h} \nabla^2 \overline{\mathbf{T}} - \dot{\overline{\mathbf{T}}} \right) = 0 \tag{6}$$

where $\mathbf{D_m}$ and $\mathbf{D_h}$ are moisture and temperature diffusivity tensors, respectively, that for isotropic media are defined as:

$$\mathbf{D_m} = \begin{bmatrix} d_m & 0 & 0 \\ 0 & d_m & 0 \\ 0 & 0 & d_m \end{bmatrix}$$

$$\mathbf{D_h} = \begin{bmatrix} d_h & 0 & 0 \\ 0 & d_h & 0 \\ 0 & 0 & d_h \end{bmatrix} \tag{7}$$

The dot superscript denotes the derivate with respect to time. Substituting Eq. (3) in Eq. (6) yields (Segerlind 1984; Liu and Quek 2003):

$$\iiint_{V^e} \mathbf{N^T} \left\{ \mathbf{D_m} \nabla^2 (\mathbf{N} \overline{\mathbf{C}}) + \lambda \mathbf{D_h} \nabla^2 (\mathbf{N} \overline{\mathbf{T}}) - \mathbf{N} \dot{\overline{\mathbf{C}}} \right\} = 0$$

$$\iiint_{V^e} \mathbf{N^T} \left\{ \nu \mathbf{D_m} \nabla^2 (\mathbf{N} \overline{\mathbf{C}}) + \mathbf{D_h} \nabla^2 (\mathbf{N} \overline{\mathbf{T}}) - \mathbf{N} \dot{\overline{\mathbf{T}}} \right\} = 0 \tag{8}$$

By using integration by parts technique and more simplifications, the final forms of Eq. (8) are derived as bellow (Segerlind 1984; Liu and Quek 2003):

$$\mathbf{k_T} \overline{\mathbf{T}} + \mathbf{k_{TC}} \overline{\mathbf{C}} - \mathbf{q_T} \dot{\overline{\mathbf{C}}} = \mathbf{f_T}$$

$$\mathbf{k_C} \overline{\mathbf{C}} + \mathbf{k_{CT}} \overline{\mathbf{T}} - \mathbf{q_C} \dot{\overline{\mathbf{T}}} = \mathbf{f_C} \tag{9}$$

In which:

$$\mathbf{k_T} = \iiint_{V^e} \mathbf{B^T D_h B} J \mathrm{d}v$$

$$\mathbf{k_{TC}} = \iiint_{V^e} \mathbf{B^T} \nu \mathbf{D_m B} J \mathrm{d}v$$

$$\mathbf{q_T} = \iiint_{V^e} \mathbf{N^T N} J \mathrm{d}v$$

$$\mathbf{k_C} = \iiint_{V^e} \mathbf{B^T D_m B} J \mathrm{d}v \tag{10}$$

$$\mathbf{k_{CT}} = \iiint_{V^e} \mathbf{B^T} \lambda \mathbf{D_h B} J \mathrm{d}v$$

$$\mathbf{q_C} = \iiint_{V^e} \mathbf{N^T N} J \mathrm{d}v$$

where J is the Jacobian of mapping from physical to references coordinate system and $\mathbf{B}$ is the shape functions derivates matrix defined as (Segerlind 1984; Liu and Quek 2003):

$$\mathbf{B} = \begin{bmatrix} \frac{\partial N_1}{\partial \xi} & \frac{\partial N_2}{\partial \xi} & \cdots & \frac{\partial N_8}{\partial \xi} \\ \frac{\partial N_1}{\partial \eta} & \frac{\partial N_2}{\partial \eta} & \cdots & \frac{\partial N_8}{\partial \eta} \\ \frac{\partial N_1}{\partial \gamma} & \frac{\partial N_2}{\partial \gamma} & \cdots & \frac{\partial N_8}{\partial \gamma} \end{bmatrix} \tag{11}$$

$\mathbf{f_T}$ and $\mathbf{f_C}$ are the force vectors of temperature and moisture elements which are due to heat and moisture generation and convection and flux boundary conditions that are not included in present work.

Finally by sweeping the matrices in Eqs. (10) for all elements and assembling them in global matrices, the global weak forms of governing equations are derived as below:

$$\mathbf{K_T T} + \mathbf{K_{TC} C} - \mathbf{M_T} \dot{\mathbf{T}} = \mathbf{F_T}$$
$$\mathbf{K_C C} + \mathbf{K_{CT} T} - \mathbf{M_C} \dot{\mathbf{C}} = \mathbf{F_C} \tag{12}$$

$\mathbf{T}$ and $\mathbf{C}$ are the vectors of global nodal unknown temperatures and moisture concentrations that want to be evaluated at any time.

Equation (12) are the sets of coupled first-order differential equations with respect to time that should be solved to evaluate the unknown nodal values of $\mathbf{T}$ and $\mathbf{C}$ at any time. By evaluation of nodal values at each time, the temperature and moisture fields can be obtained at any space coordinates (r, θ, z) and time t.

4 Time Integration Scheme

In this work, the resulted sets of differential equations [Eq. (12)] are solved numerically by using Runge–Kutta method (Chan et al. 2003). At first Eq. (12) should be rearranged as:

$$\dot{\mathbf{T}} = \mathbf{Q_T^{-1}} \left(\mathbf{K_T T} + \mathbf{K_{TC} C} - \mathbf{F_T} \right)$$
$$\dot{\mathbf{C}} = \mathbf{Q_C^{-1}} \left(\mathbf{K_C C} + \mathbf{K_{CT} T} - \mathbf{F_C} \right) \tag{13}$$

The fourth-order Runge–Kutta method for Eq. (13) is developed as follow (Chan et al. 2003):

$$
\begin{aligned}
\mathbf{k_1} &= \Delta t\left\{-\mathbf{Q_T^{-1}K_{CT}}\left(^{i-1}\mathbf{C}\right)-\mathbf{Q_T^{-1}K_T}\left(^{i-1}\mathbf{T}\right)+\mathbf{Q_T^{-1}F_T}\right\} \\
\mathbf{l_1} &= \Delta t\left\{-\mathbf{Q_C^{-1}K_C}\left(^{i-1}\mathbf{C}\right)-\mathbf{Q_T^{-1}K_{TC}}\left(^{i-1}\mathbf{T}\right)+\mathbf{Q_T^{-1}F_C}\right\} \\
\mathbf{k_2} &= \Delta t\left\{-\mathbf{Q_T^{-1}K_{CT}}\left(^{i-1}\mathbf{C}+0.5\mathbf{l_1}\right)-\mathbf{Q_T^{-1}K_T}\left(^{i-1}\mathbf{T}+0.5\mathbf{k_1}\right)+\mathbf{Q_T^{-1}F_T}\right\} \\
\mathbf{l_2} &= \Delta t\left\{-\mathbf{Q_C^{-1}K_C}\left(^{i-1}\mathbf{C}+0.5\mathbf{l_1}\right)-\mathbf{Q_T^{-1}K_{TC}}\left(^{i-1}\mathbf{T}+0.5\mathbf{k_1}\right)+\mathbf{Q_T^{-1}F_C}\right\} \\
\mathbf{k_3} &= \Delta t\left\{-\mathbf{Q_T^{-1}K_{CT}}\left(^{i-1}\mathbf{C}+0.5\mathbf{l_2}\right)-\mathbf{Q_T^{-1}K_T}\left(^{i-1}\mathbf{T}+0.5\mathbf{k_2}\right)+\mathbf{Q_T^{-1}F_T}\right\} \\
\mathbf{l_3} &= \Delta t\left\{-\mathbf{Q_C^{-1}K_C}\left(^{i-1}\mathbf{C}+0.5\mathbf{l_2}\right)-\mathbf{Q_T^{-1}K_{TC}}\left(^{i-1}\mathbf{T}+0.5\mathbf{k_2}\right)+\mathbf{Q_T^{-1}F_C}\right\} \\
\mathbf{k_4} &= \Delta t\left\{-\mathbf{Q_T^{-1}K_{CT}}\left(^{i-1}\mathbf{C}+\mathbf{l_3}\right)-\mathbf{Q_T^{-1}K_T}\left(^{i-1}\mathbf{T}+\mathbf{k_3}\right)\mathbf{Q_T^{-1}F_T}\right\} \\
\mathbf{l_4} &= \Delta t\left\{-\mathbf{Q_C^{-1}K_C}\left(^{i-1}\mathbf{C}+\mathbf{l_3}\right)-\mathbf{Q_T^{-1}K_{TC}}\left(^{i-1}\mathbf{T}+\mathbf{k_3}\right)+\mathbf{Q_T^{-1}F_C}\right\}
\end{aligned}
\tag{14}
$$

$$
\begin{aligned}
^i\mathbf{T} &= {^{i-1}\mathbf{T}}+\frac{1}{6}\left(\mathbf{k_1}+2\mathbf{k_2}+2\mathbf{k_3}+\mathbf{k_4}\right) \\
^i\mathbf{C} &= {^{i-1}\mathbf{C}}+\frac{1}{6}\left(\mathbf{l_1}+2\mathbf{l_2}+2\mathbf{l_3}+\mathbf{l_4}\right)
\end{aligned}
\tag{15}
$$

where Δt is the time step, and $k_j (j = 1 \dots 4)$ and $l_j (j = 1 \dots 4)$ are the Runge–Kutta formulation parameters. Equations (14) and (15) starts from $i = 2$ and $i = 1$ corresponding to initial conditions of temperature and moisture. Using the above algorithm, the nodal values of temperature and moisture can be obtained directly at any time.

5 Result and Discussion

In this section, for all cases, the temperatures and moisture concentrations at any locations are denoted by T and C, respectively. Also, the temperature is in centigrade and the moisture concentration has $\left(\frac{kg}{cm^3}\right)$ unites.

5.1 Comparison Study

In this work for the validity of presented FEM formulation, the used time integration scheme (generalized fourth-order Runge–Kutta method), and four examples from other literature are selected and presented here and the results of present model are compared with them.

Case 1 The first example is an infinitely long cylinder under thermal gradient (one-dimensional heat conduction problem in cylindrical coordinate), for both temperature and convection boundary conditions. This steady-state problem is solved analytically, and also the same results are prepared with the present FEM method and are reported in Tables 1 and 2. It should be noted that, for the steady-state problem of heat conduction and related boundary conditions, a closed-form solution in the references and the comparison between the results of FEM and analytical solutions is very appropriate to verify the present model.

For this example, the geometrical parameters of cylinder are as follow:

Table 1 Temperature distribution in radial direction for a long cylinder with boundary conditions of case (a)

R (m)	1	1.1	1.2	1.3	1.4	1.5
Present FEM	50	85.2592	117.4485	147.0600	174.4761	200
Analytical solution	50	85.2598	117.4490	147.0605	174.4764	200

Table 2 Temperature distribution in radial direction for a long cylinder with boundary conditions of case (b)

R (m)	1	1.1	1.2	1.3	1.4	1.5
Present FEM	50	83.0837	113.2868	141.0709	166.7950	190.7436
Analytical solution	50	83.0833	113.2861	141.0703	166.7945	190.7433

$$a = 1, \quad b = 1.5$$

And reduced heat conduction equation for this case and boundary conditions are:

$$\frac{\partial^2 T}{\partial r^2} = 0$$

(a) Inner and outer surfaces are in constant temperature conditions as:

$$r = a \rightarrow T = T_i = 50$$
$$r = b \rightarrow T = T_o = 100$$

(b) Inner surface is in constant temperature and outer surface is in convection boundary conditions as:

$$r = a \rightarrow T = T_i = 50$$
$$r = b \rightarrow -k\frac{\partial T}{\partial r} = h(T - T_\infty)$$

where

$$h = 5\frac{\text{W}}{\text{m}^2 \text{ K}}$$
$$T_\infty = 200$$

From Tables 1 and 2, a very good agreement between the present FEM model and analytical solutions is observed for both different boundary conditions.

Case 2 A cylinder of finite length but in axisymmetric condition (two-dimensional heat transfer problem) is considered as the second example, and the temperature distributions in the cylinder are computed using present FEM model, and also the results are obtained by ANSYS software and reported in Table 3. For ANSYS simulation, the PLANE77 is used, this element has 8 nodes and one degree of freedom, temperature, at each node.

Table 3 Temperature distribution for an axisymmetric cylinder with finite length

(r, z)	$(1.3, 0)$	$(1.1, 1.8)$	$(1.2, 0.6)$	$(1.3, 1.5)$	$(1.3, 1.2)$	$(1.5, 1.8)$
Present FEM	-64.3369	104.8918	106.6360	145.7030	141.6638	195.1811
ANSYS	-64.2650	103.2000	106.5900	145.5400	141.6300	195.1500

The heat conduction equation corresponding to case 2 is as follows:

$$\frac{\partial^2 T}{\partial r^2} + \frac{\partial^2 T}{\partial z^2} = 0$$

The geometrical dimensions and boundary conditions parameters for this example are as bellow:

$$a = 1, \quad b = 1.5, \quad L = 2$$

and,

$$r = a \rightarrow T = 50$$
$$r = b \rightarrow h = 5, T_\infty = 200$$
$$z = 0 \rightarrow h = 5, T_\infty = -100$$
$$z = L \rightarrow T = 200$$

Case 3 As a three-dimensional comparison case, a cylinder with nonaxisymmetric boundary conditions is considered as the third example and the temperature distributions in the whole volume of a cylinder are obtained with present FEM model and also with ANSYS. For ANSYS simulation, the SOLID279 is used, SOLID279 is a higher-order 3D 20-noded solid element that exhibits quadratic thermal behavior. The geometrical dimension and boundary conditions parameters and 3D heat conduction equation are as follow:

$$a = 0.1, \quad b = 0.3, \quad L = 0.5$$
$$\frac{\partial^2 T}{\partial r^2} + \frac{1}{r^2}\frac{\partial^2 T}{\partial \theta^2} + \frac{\partial^2 T}{\partial z^2} = 0$$

and

$$r = a \rightarrow T = 50, \quad r = b \rightarrow T = 0$$
$$Z = 0 \rightarrow T = 0, \quad Z = L \rightarrow \begin{cases} T = 100 \rightarrow 0 \leq \theta < \pi \\ T = 200 \rightarrow \pi \leq \theta < 2\pi \end{cases}$$

The obtained results are shown in Table 4.

Tables 3 and 4 show that the present FEM model is a very accurate method for two- and three-dimensional steady-state heat conductions of cylinders under various boundary conditions; also, these results are valid for steady state moisture distributions because the differential equations that govern the heat conduction and moisture diffusion are the same in nature and only the coefficients and parameters are different. These results show the capacity of the FEM model to analyze various shapes of cylinders and also various boundary conditions in the steady-state heat conduction and moisture distributions.

Table 4 Temperature distribution for a three-dimensional cylinder

(r, θ, z)	(0.2, 0, 0.1)	(0.28, π/4,0.35)	(0.2,5π/6,0.4)	(0.15,3π/2,0.4)	(0.15, π/3,0.4)
Present FEM	13.9025	5.8936	41.1900	69.8469	48.5112
ANSYS	13.9110	6.0496	42.728	69.6980	48.7610
(r, θ, z)	(0.27,3π/2,0.4)	(0.2,3π/2,0.48)	(0.2, π/3,0.48)	(0.2, π/2,0.1)	(0.2,3π/2,0.3)
Present FEM	25.5900	165.6121	84.5972	13.8375	28.6098
ANSYS	25.7350	165.10	84.464	13.803	28.470

Case 4 All of the above examples are in steady-state and uncoupled conditions, in the fourth example the transient coupled temperature and moisture diffusion in a one-dimensional bar of a porous material is analyzed with present FEM method and compared with the results presented by Sih et al. (1986).

The material properties and coupling coefficients of the porous material are:

$$\lambda = 0.122 \frac{\text{kg}}{\text{m}^3\,\text{K}}, \quad \nu = 2.53 \frac{\text{m}^3\,\text{K}}{\text{kg}}$$

$$D_{\text{m}} = 9.2 \times 10^{-7} \text{ cm}^2/\text{hr}, \quad D_{\text{h}} = 9.2 \times 10^{-6} \text{ cm}^2/\text{hr},$$

And the boundary and initial conditions are as follow:

$$T(0, x) = 0;$$
$$C(0, x) = 0;$$
$$T(t, 0) = T(t, L) = T_f$$
$$C(t, 0) = C(t, L) = C_f$$

The dimensionless time parameter is defined as:

$$S = \sqrt{(1 - \lambda\nu)D_{\text{h}}t/H^2}$$

For this example, the normalized results are presented in Figs. 3 and 4 for various time parameters *S*.

From Figs. 3 and 4, it is obvious that the presented FEM model and also the used time integration scheme give the results which are very close to the analytical results obtained by Sih et al. (1986). Figures 3 and 4 show that the present coupled FEM model can be used to simulate the static and dynamic problems, and also this model has a very acceptable accuracy.

5.2 Coupled Heat and Moisture Transfer in Cylinders, $\alpha = 2\pi$ (Axisymmetric Condition)

In the case of axially symmetric conditions, there are no temperature and moisture changes in the circumferential direction (θ), and so the results are derived from the present model in the plane ($\theta = 0$).The geometrical parameters in this section are as follows:
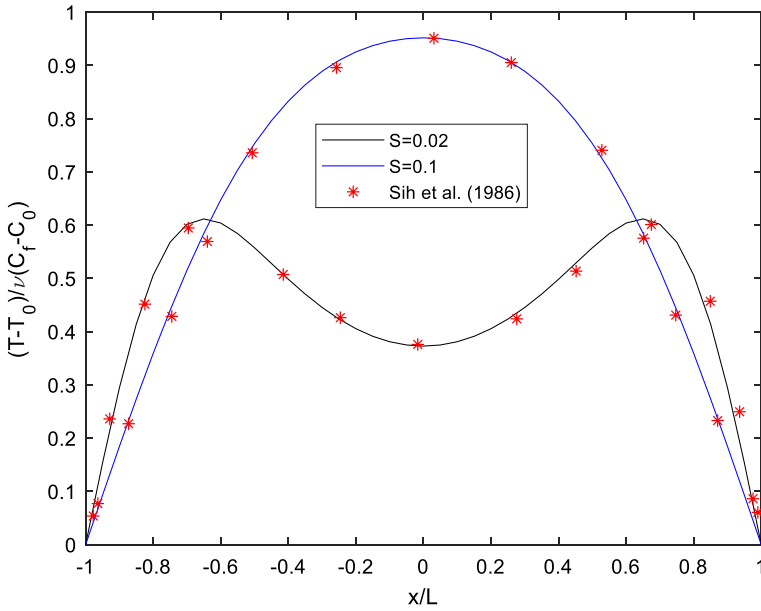
Fig. 3 Normalized temperature distributions for various time parameter (S)
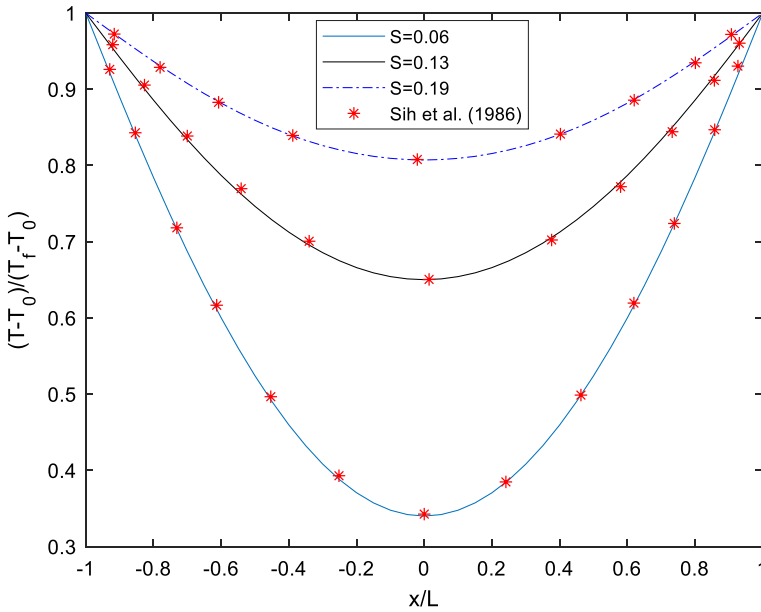
Fig. 4 Normalized temperature distributions for various time parameter (S)

Table 5 Temperature and moisture distribution at time parameter $t^* = 0.0138$

Location, (r, z)	(1.2, 1)	(1.1, 3)	(1.3, 2)	(1.3, 4)	(1.5, 1)
T	64.3357	80.3125	52.8074	53.0877	43.3622
C	7.1376	5.0376	6.8693	6.8993	5.7080
Location, (r, z)	(1.5, 4)	(1.5, 2.5)	(1.8, 1)	(1.9, 3)	(1.9, 4.5)
T	43.5952	43.1705	58.0238	68.4626	71.8432
C	5.7311	5.6829	6.4099	4.2525	4.2212

Table 6 Temperature and moisture distribution at time parameter $t^* = 0.0276$

Location, (r, z)	(1.2, 1)	(1.1, 3)	(1.3, 2)	(1.3, 4)	(1.5, 1)
T	80.8716	89.9474	75.3539	75.1779	68.0447
C	7.6758	4.7113	9.0370	9.0146	8.9502
Location, (r, z)	(1.5, 4)	(1.5, 2.5)	(1.8, 1)	(1.9, 3)	(1.9, 4.5)
T	68.8632	68.9808	71.6370	75.8776	76.9951
C	9.0549	9.0733	6.6909	3.8572	3.4281

$$a = 1, \quad b = 2, \quad L = 5$$

Case 1 In this case, the coupled heat and moisture transfer in the axially symmetric conditions is obtained. The boundary conditions are as follow:

$$T_i = 100, \quad T_o = 80, \quad T_t = 20, \quad T_b = 0, \quad C_i = C_o = C_t = C_b = 0$$

Subscripts i, j, t and b referred to inner, outer, top and bottom surfaces of cylinder, respectively. For all examples of this work, the initial temperature and moisture distributions are supposed to be zero.

Tables 5 and 6 show the temperature and moisture at some point locations of the cylinder for two different time parameters.

The time parameter t^* is defined as:

$$t^* = \frac{d_m(1 - \lambda v)t}{a^2}$$

Tables 5 and 6 show that temperature changes in the cylinder make a significant change in the moisture content of the cylinder and both moisture and temperature transfers from high-temperature zones to low-temperature zones.

Case 2 In this case, a cylinder with geometrical dimensions which are the same as previous example, and following end conditions is considered:

$$C_i = 30, \quad C_o = 20, \quad C_t = 40, \quad C_b = 0, \quad T_i = T_o = T_t = T_b = 0$$

Table 7 Temperature and moisture distribution for a cylinder at various time parameters

t^*		Location (r, z)					
		(1.2, 1)	(1.2, 4)	(1.5, 0.7)	(1.5, 4.5)	(1.9, 2)	(1.8, 3.5)
0.0414	T	3.5351	3.8418	4.1582	5.3719	1.5520	2.9119
0.0414	C	9.7087	9.7157	1.1240	5.1867	13.2190	7.5335
0.0828	T	2.7965	3.1584	3.6432	4.2755	1.2197	2.3985
0.0828	C	13.9220	13.8060	4.4777	11.0500	15.1920	10.7820
0.0966	T	2.5893	2.9487	3.3870	3.8942	1.1340	2.2423
0.0966	C	14.8870	14.7850	5.6674	12.799	15.5970	11.5200
Steady state	T	2.4559	2.8104	3.2117	3.6454	1.0795	2.1406
Steady state	C	15.4980	15.4190	6.4687	13.930	15.8490	11.9890

The results are presented in Table 7 for various time parameters and also for steady state condition.

From Table 7, it is observed that the moisture change makes an important change in temperature distribution in a cylinder. Also as the time passes, both temperature and moisture at all locations converge to steady-state values, that is an expected conclusion and confirm the correctness of proposed model results. It can be seen from Table 7 that, as the time parameter increases, in the same location, the value of the temperature decreases, but the moisture increases. This result is similar to physical anticipation from the distribution of temperature and moisture during the time.

For more resolution of variation of temperature and moisture with time, in the following examples (cases 3 and 4) an axisymmetric cylinder with coupled and uncoupled conditions is considered.

Case 3 In this case at the boundary of the cylinder, the temperature is kept at zero and a constant moisture concentration is applied to the boundary.

The geometrical dimensions and boundary conditions are as below:

$$a = 1, \quad b = 1.5, \quad L = 2$$

and

$$C_i = 30, \quad C_o = 0, \quad C_t = 40, \quad C_b = 20, \quad T_i = T_o = T_t = T_b = 0$$

Figures 5 and 6 show the time history of moisture concentration at two different locations of the cylinder for both coupled and uncoupled conditions, it should be pointed out that the uncoupled results for both temperature and moisture are obtained by putting $\lambda = v = 0$ in the formulations.

Case 4 In this example, the moisture concentrations at the boundaries of the cylinder are kept to zero and constant temperature is prescribed at the surfaces of cylinder. Geometrical and boundary conditions of this case are as follows:
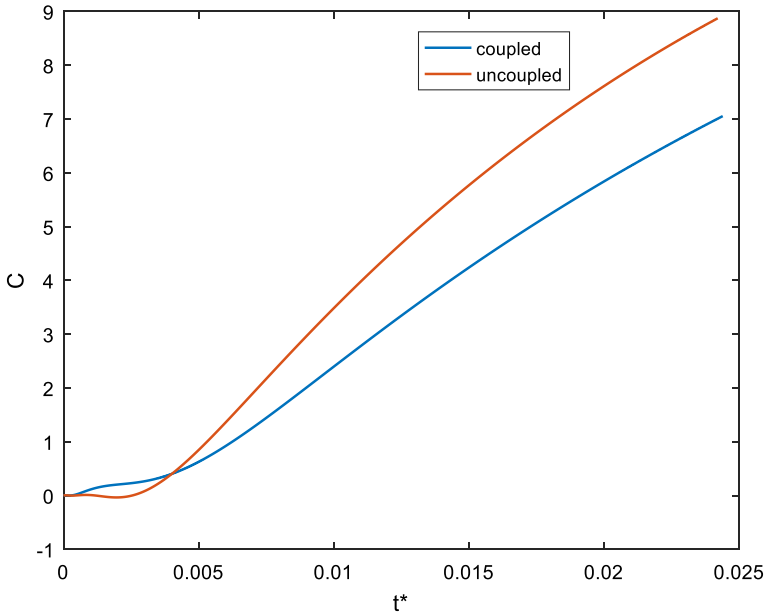
Fig. 5 Time history of moisture concentration for a point at location $(r, \theta, z) = (1.25, 0, 1.33)$
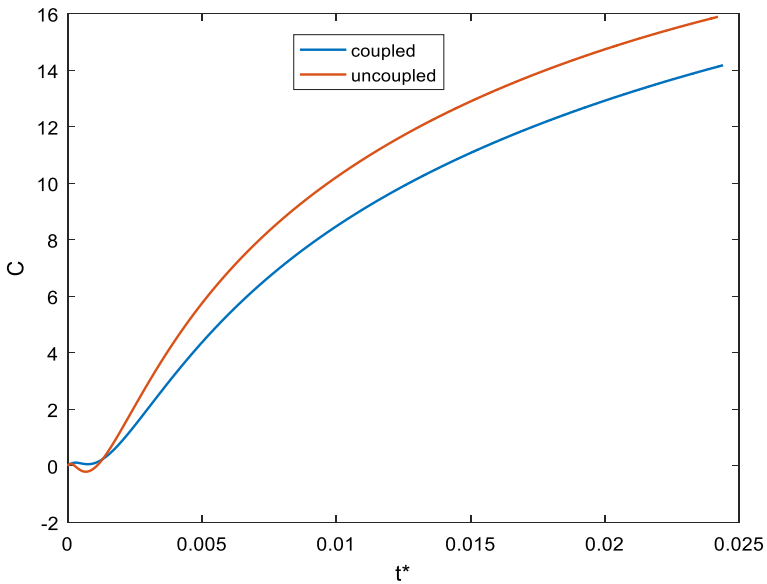
Fig. 6 Time history of moisture concentration for a point at location $(r, \theta, z) = (1.5, 0, 0.533)$

$$a = 1, \quad b = 1.5, \quad L = 2$$

$$T_i = 100, \quad T_o = 0, \quad T_t = 40, \quad T_b = 30, \quad C_i = C_o = C_t = C_b = 0$$
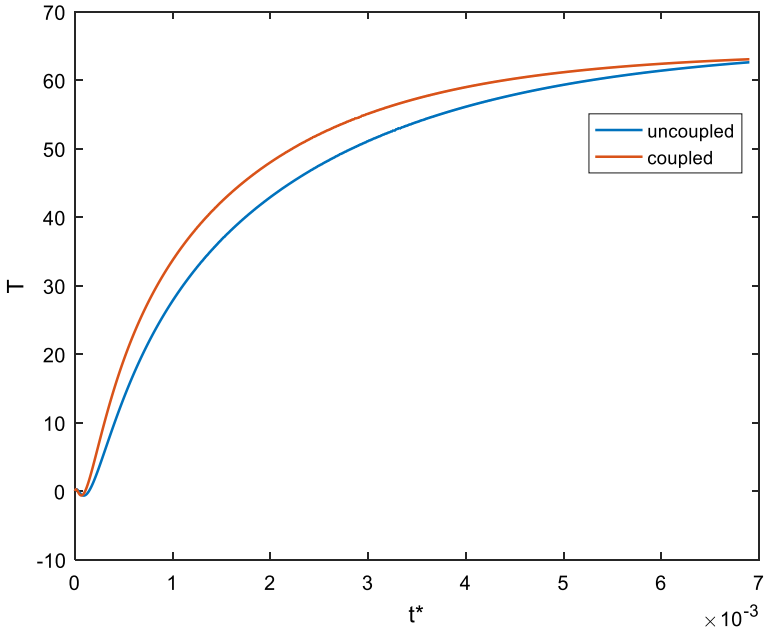
Fig. 7 Time history of temperature for a point at location $(r, \theta, z) = (1.5, 0, 0.533)$
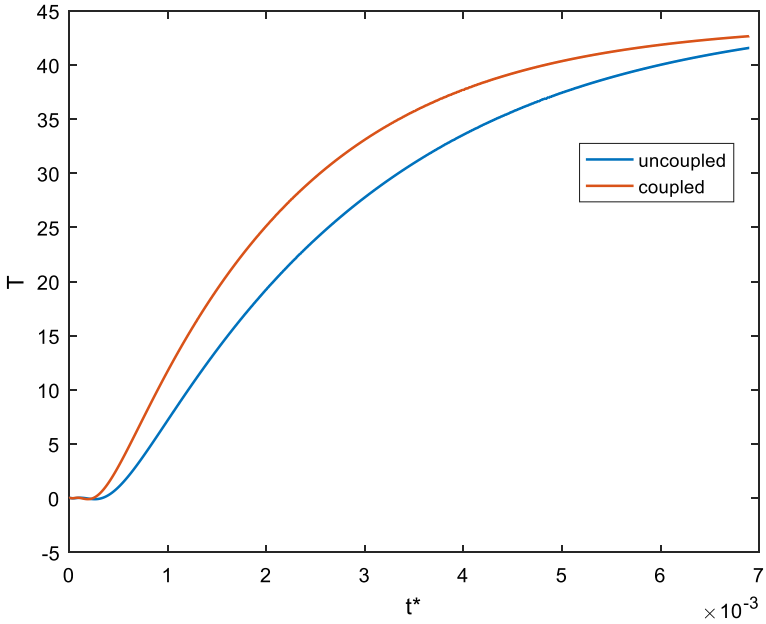
Fig. 8 Time history of temperature for a point at location $(r, \theta, z) = (1.25, 0, 1.33)$

Figures 7 and 8 show the time history of temperature at two different locations of the cylinder for both coupled and uncoupled solutions.

From these figures, it is obvious that at a short interval of time at the beginning of diffusion process the uncoupled results are higher than the coupled ones and with the passage of time this pattern is changed and the coupled results become higher than the coupled ones. Also, it can be seen that during the time the values of coupled and uncoupled temperatures converge to each other, whereas for moisture concentration during the time, these values diverge from each other according to Figs. 5 and 6. Also, Figs. 7 and 8 show a similar qualitative variation for the time history of temperature by changing the point of location in the axial direction.

5.3 Coupled Heat and Moisture Transfer in a Cylinder, $\alpha = 2\pi$ (Non-axisymmetric Condition)

In this part, a cylinder of geometrical dimensions of ($a = 0.5$, $b = 0.7$ and $L = 0.5$) is considered under following boundary conditions:

$$T_i = 0$$
$$T_o = 100$$
$$T_b = 0$$
$$T_t = \begin{cases} 60 \rightarrow 0 \leq \theta < \pi \\ -40 \rightarrow \pi \leq \theta < 2\pi \end{cases}$$
$$C_i = C_o = C_t = C_b = 0$$

As can be seen, the prescribed temperature boundary condition on the top surface of the cylinder is not symmetric and so the temperature and moisture varied along the circumferential direction (θ), and the problem is fully three dimensional.

Figures 9 and 10 show the contour plots of moisture concentration distribution at plane ($z = 0.9L$) of the cylinder. These figures show that applying unsymmetrical boundary condition causes unsymmetrical temperature and moisture distributions in the cylinder. Also at the zone of higher temperature, the moisture concentration is higher than those of lower temperature.

Distribution of temperature at plane ($\theta = 0$) is illustrated in Fig. 11, and this figure is a very good representation of the diffusion of heat from higher temperature to lower temperature zones.

Also, Figs. 12 and 13 show the contours of moisture concentration at two different times. From these figures, it can be seen that with the passage of time in spite of temperature diffusion in Fig. 11, the moisture concentration moved as an aggregate of moisture from higher temperature to lower temperature zones. These phenomena can be justified by regarding this fact that the moisture diffusion is actually the transfer of mass and by considering the principle of conservation of mass the moisture content of medium should be displaced from one position to another.

It can be seen from Figs. 9, 10, 11, 12, and 13 that, the present model can simulate the hygro-thermal phenomenon in the 3D mechanical structures. Prediction of the distribution of temperature and moisture concentration in 3D is very important in structures with hygro-thermal environments, and the results of this paper can be used to predict the mechanical properties of the cylindrical shells under coupled thermal and moisture effect.
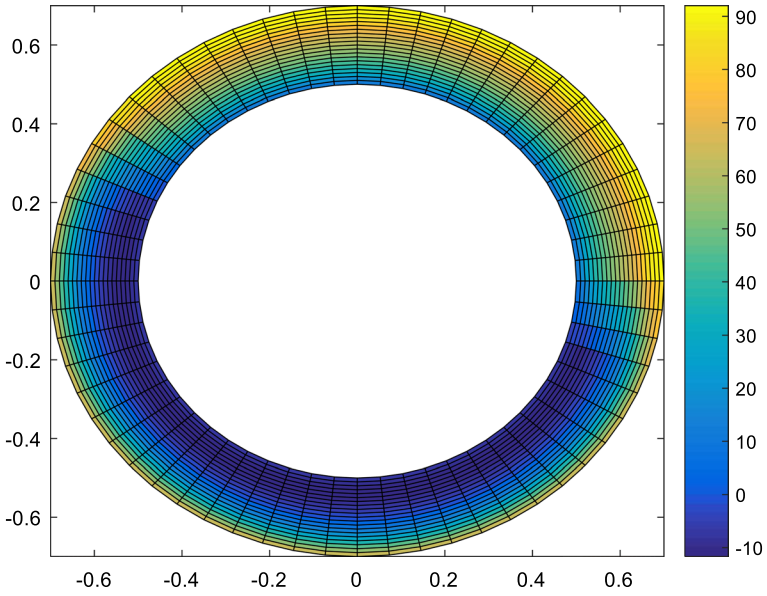
Fig. 9 Contour of temperature at time parameter ($t^* = 0.138$), $z{=}0.9L$
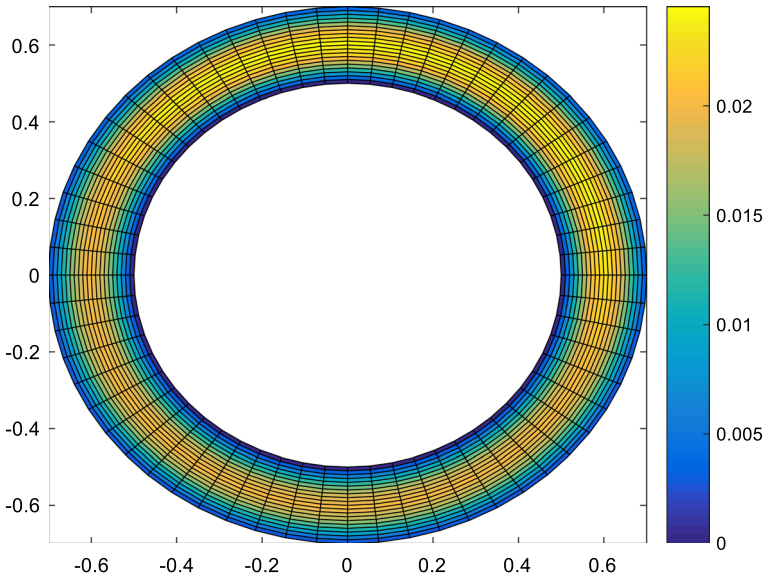
Fig. 10 Contour of moisture concentration at time parameter ($t^* = 0.138$), $z{=}0.9L$

5.4 Coupled Heat and Moisture Transfer in Cylindrical Panels ($\alpha = \pi/4$)

In this section, a cylindrical panel with the following geometrical dimensions is considered:
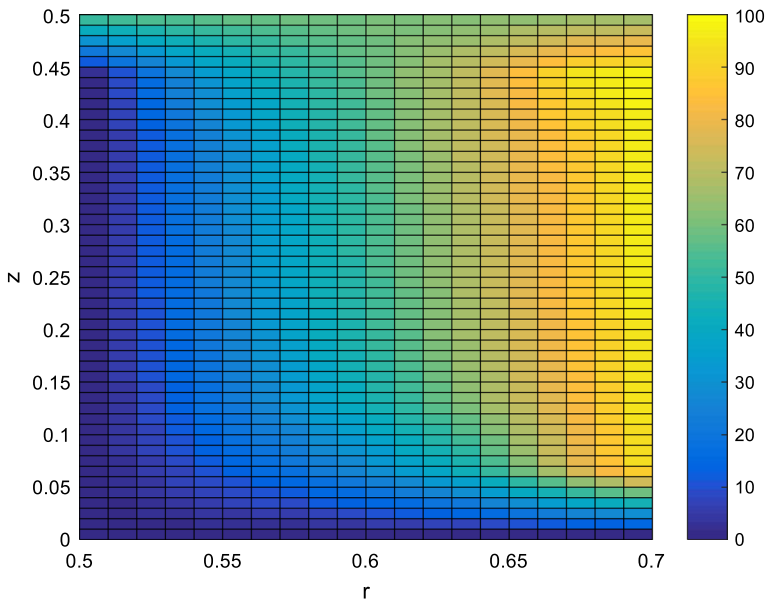
Fig. 11 Contour of temperature at time parameter ($t^* = 0.138$), $\theta = 0$
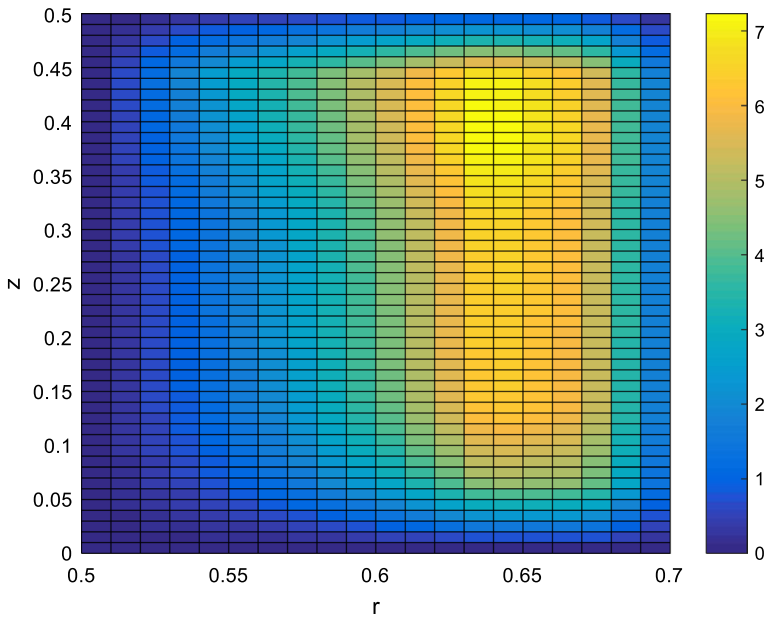
Fig. 12 Contour of moisture concentration at time parameter ($t^* = 0.0028$), $\theta = 0$
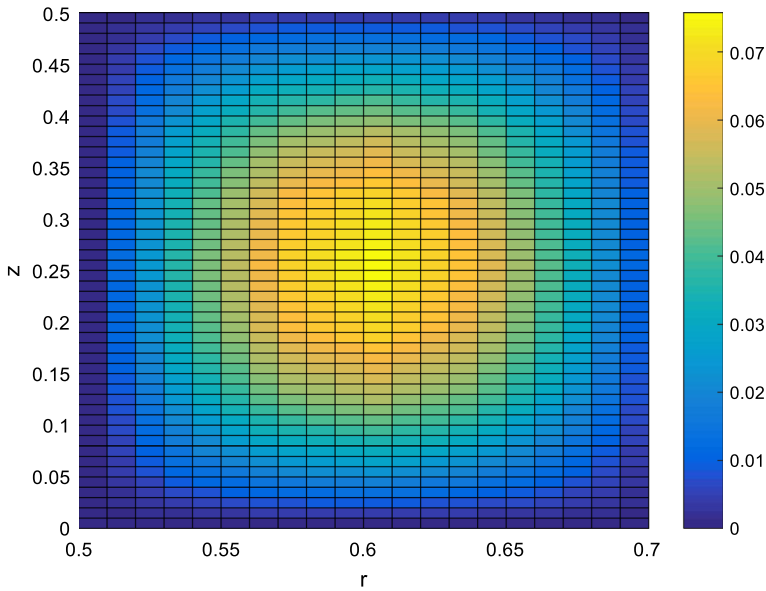
Fig. 13 Contour of moisture concentration at time parameter ($t^* = 0.138$), $\theta = 0$

$$a = 0.5, \quad b = 0.7, \quad L = 0.5, \quad \alpha = \frac{\pi}{4}$$

In the inner surface of the panel, the inner temperature of $T_i = 100$ is prescribed and all other boundaries are kept at zero for temperatures and moisture concentrations.

Figures 14 to 17 show the contours of temperature and moisture at two different time parameters at the middle surface of the panel in the circumferential direction. Also, the contour of temperature and moisture at the middle plane of the panel in the axial direction is illustrated in Figs. 18 and 19.

Figures 14, 15, 16, 17, 18, and 19 show the same results for a full cylinder. By applying temperature difference to panel, the moisture transfers from high-temperature zones to low zones and with the passing of time, it is observed that the moisture content of panel moves as an aggregate of moisture from one zone to another.

6 Conclusion

In this work, transient coupled heat and moisture transfer are performed in the cylindrical panels of porous medium with three-dimensional finite element methods. The cylindrical elements are used, and Runge–Kutta method is developed to solve the systems of governing differential equations.

It is concluded that the used finite element formulation is a very accurate and powerful method to the analysis of coupled heat and moisture transfer.

Also, the results show that applying temperature differences to a porous medium make a significant change in the moisture distributions and applying moisture differences make a significant change in temperature distributions that reveal the importance of coupled
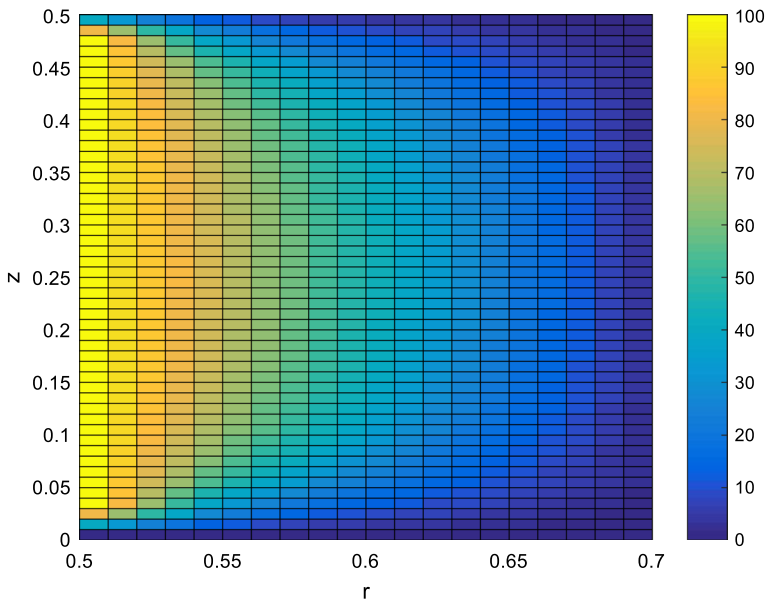
Fig. 14 Contour of temperature at time parameter ($t^* = 0.0138$), $\theta = \frac{\alpha}{2}$
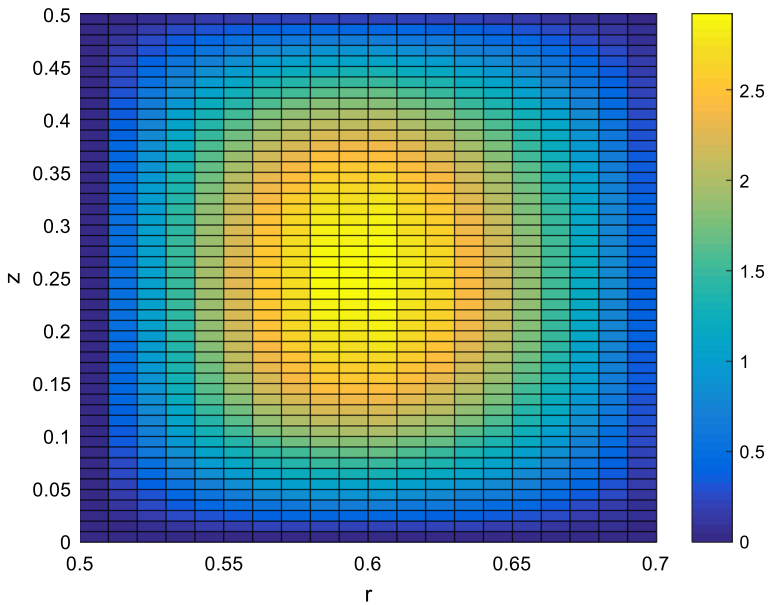
Fig. 15 Contour of moisture concentration at time parameter ($t^* = 0.0138$), $\theta = \frac{\alpha}{2}$

analysis in highly accurate applications. Another conclusion is that during the time the values of coupled and uncoupled temperatures converge to each other whereas for moisture concentration during the time these values diverge from each other.
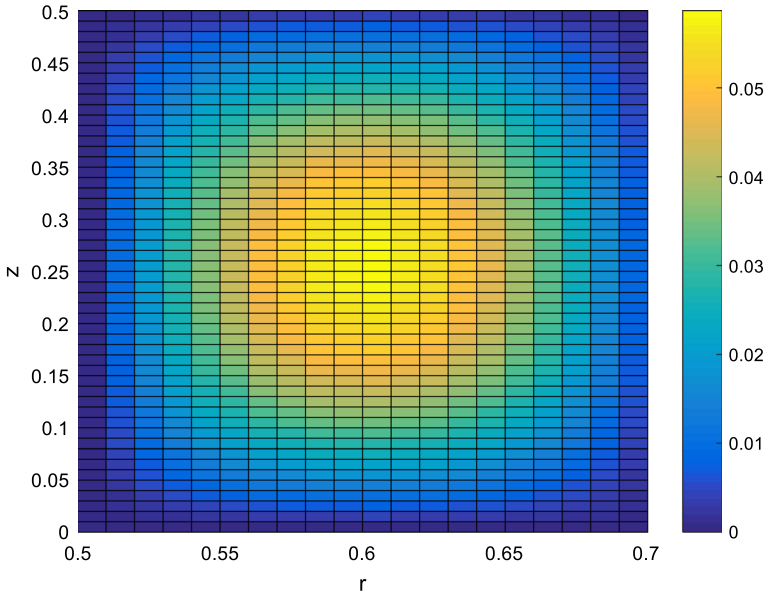
Fig. 16 Contour of moisture concentration at time parameter ($t^* = 0.138$), $\theta = \frac{\alpha}{2}$
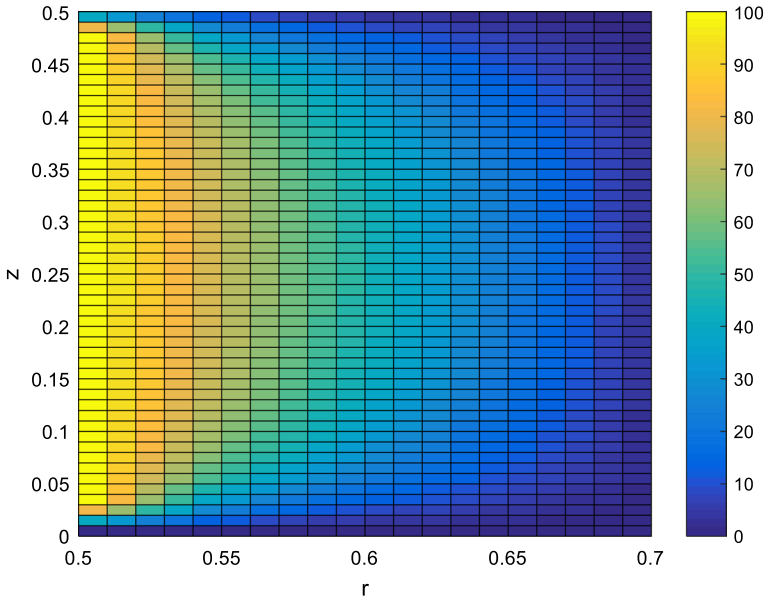
Fig. 17 Contour of temperature at time parameter ($t^* = 0.138$), $\theta = \frac{\alpha}{2}$

From contour plots, it is observed that by applying temperature on the cylinder surfaces the moisture content of the cylinder moves as an aggregate of moisture from one position to another.
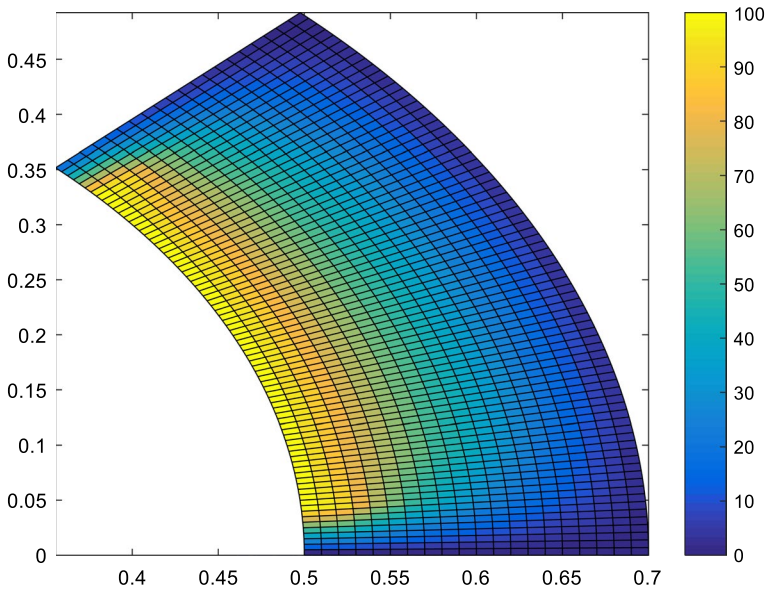
Fig. 18 Contour of temperature at time parameter ($t^* = 0.138$), $z = \frac{L}{2}$
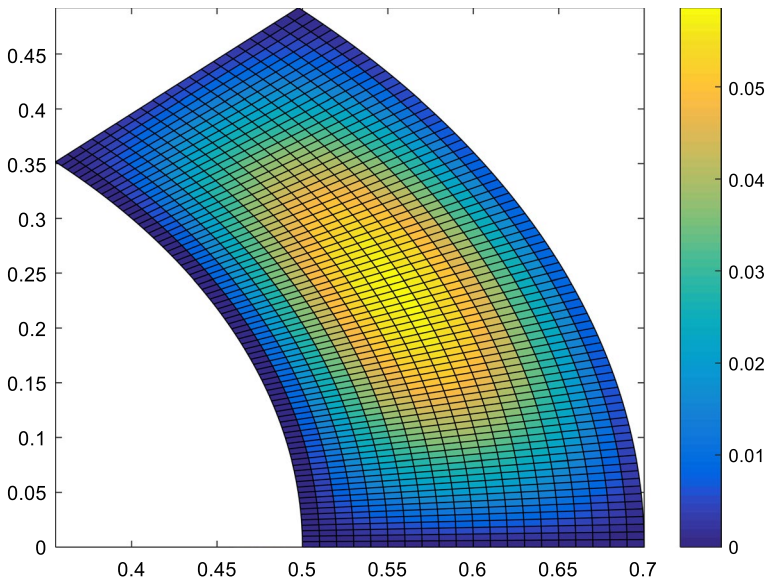
Fig. 19 Contour of moisture concentration at time parameter ($t^* = 0.138$), $z = \frac{L}{2}$

References

Arefi, M., Firouzeh, S., Bidgoli, E.M.R., Civalek, O.: Analysis of porous micro-plates reinforced with FG-GNPs based on Reddy plate theory. Compos. Struct. **247**(1), 112391 (2020)

Bisheh, H., Civalek, O.: Vibration of smart laminated carbon nanotube-reinforced composite cylindrical panels on elastic foundations in hygrothermal environments. Thin-Walled Struct. **155**, 106945 (2020)

Chan, M.F.C.F., De Kee, D., Kaloni, P.N.: Advanced Mathematics for Engineering and Science. World Scientific, Singapore (2003)

Chang, W.-J.: Transient hygrothermal responses in a solid cylinder by linear theory of coupled heat and moisture. Appl. Math. Model. **18**, 467–473 (1994)

Chang, W.-J., Weng, C.-I.: An analytical solution to coupled heat and moisture diffusion transfer in porous materials. Int. J. Heat Mass Trans. **43**, 3621–3632 (2000)

Cinefra, M., Petrolo, M., Li, G., Carrera, E.: Hygrothermal analysis of multilayered composite plates by variable kinematic finite elements. J. Therm. Stress. **40**, 1502–1522 (2017a)

Cinefra, M., Petrolo, M., Li, G., Carrera, E.: Variable kinematic shell elements for composite laminates accounting for hygrothermal effects. J. Therm. Stress. **40**, 1523–1544 (2017b)

Dastjerdi, S., Beni, Y.T.: A novel approach for nonlinear bending response of macro-and nanoplates with irregular variable thickness under nonuniform loading in thermal environment. Mech. Based Des. Struct. Mach. **47**, 453–478 (2019)

Dastjerdi, S., Akgöz, B., Civalek, O.: On the effect of viscoelasticity on behavior of gyroscopes. Int. j. Eng. Sci. **149**, 103236 (2020b)

Dastjerdi, S., Beni, Y.T., Malikan, M.: A comprehensive study on nonlinear hygro-thermo-mechanical analysis of thick functionally graded porous rotating disk based on two quasi-three-dimensional theories. Mech. Based Des. Struct. Mach. (2020a). https://doi.org/10.1080/15397734.2020.1814812

Dastjerdi, S., Malikan, M., Dimitri, R., Tornabene, F.: Nonlocal elasticity analysis of moderately thick porous functionally graded plates in a hygro-thermal environment. Compos. Struct. **255**, 112925 (2021)

Fallahi, N., Viglietti, A., Carrera, E., Pagani, A., Zappino, E.: Effect of fiber orientation path on the buckling, free vibration, and static analyses of variable angle tow panels. Facta Universitatis, Ser.: Mech. Eng. **18**(2), 165–188 (2020)

Fick, A.: Ueber diffusion. Ann. Phys. **94**, 59–91 (1855)

Genao, F.Y., Kim, J., Żur, K.K.: Nonlinear finite element analysis of temperature-dependent functionally graded porous micro-plates under thermal and mechanical loads. Compos. Struct. **256**, 112931 (2021)

Ghobadi, A., Beni, Y.T., Żur, K.K.: Porosity distribution effect on stress, electric field and nonlinear vibration of functionally graded nanostructures with direct and inverse flexoelectric phenomenon. Compos. Struct. **259**(1), 113220 (2021)

Incropera, F.P., De Witt, D.P., Bergman, T.L., Lavine, A.S.: Introduction to Heat Transfer, 5th edn. Wiley, Hoboken (2006)

Jalaei, M.H., Civalek, Ö: On dynamic instability of magnetically embedded viscoelastic porous FG nanobeam. Int. j. Eng. Sci. **143**, 14–32 (2019)

Jankowski, P., Żur, K.K., Kim, J., Reddy, J.N.: On the bifurcation buckling and vibration of porous nanobeams. Compos. Struct. **250**, 112632 (2020)

Kim, J., Żur, K.K., Reddy, J.N.: Bending, free vibration, and buckling of modified couples stress-based functionally graded porous micro-plates. Compos. Struct. **209**, 879–888 (2019)

Kumar, J.S., Chakraverty, S., Malikan, M., Sedighi, H.M.: Hygro-magnetic vibration of the single-walled carbon nanotube with nonlinear temperature distribution based on a modified beam theory and nonlocal strain gradient model. Int. j. Appl. Mech. **12**(05), 2050054 (2020)

Lai, W.M., Krempl, E., Rubin, D.: Introduction to Continuum Mechanics, 4th edn. Butterworth-Heinemann, Burlington (2010)

Liu, G.R., Quek, S.S.: The Finite Element Method: A Practical Course. Butterworth-Heinemann, Burlington (2003)

Lv, Z., Liu, P., Zhao, Y.: Experimental study on the effect of gas adsorption on the effective stress of coal under triaxial stress. Transp. Porous Media **137**, 365–379 (2021)

Ma, X., Cheng, B., Mao, J., Liu, W., Zi, D.: Finite element modelling of coupled heat and moisture transfer in typical earth-sheltered building envelope. In: Eleventh International IBPSA Conference, pp. 1850–1856 (2009)

Malekzadeh Fard, K., Pourmoayed, A.R.: Optimization of the prismatic core sandwich panel under buckling load and yield stress constraints using an improved constrained differential evolution algorithm. J. Appl. Comput. Mech. **6**(4), 920–933 (2020)

Noori, A.R., Aslan, T.A., Temel, B.: Dynamic analysis of functionally graded porous beams using complementary functions method in the Laplace domain. Compos. Struct. **256**, 113094 (2021)

Saadatfar, M.: Stress redistribution analysis of piezomagnetic rotating thick-walled cylinder with temperature- and moisture-dependent material properties. J. Appl. Comput. Mech. **6**(1), 90–104 (2020)

Salehipour, H., Shahsavar, A., Civalek, O.: Free vibration and static deflection analysis of functionally graded and porous micro/nanoshells with clamped and simply supported edges. Compos. Struct. **221**(1), 110842 (2019)

Salehipour, H., Shahgholian-Ghahfarokhi, D., Shahsavar, A., Civalek, O., Edalati, M.: Static deflection and free vibration analysis of functionally graded and porous cylindrical micro/nano shells based on the three-dimensional elasticity and modified couple stress theories. Mech. Based Des. Struct. Mach. (2020). https://doi.org/10.1080/15397734.2020.1775095

Segerlind, L.J.: Applied Finite Element Analysis, 2nd edn. Wiley, Toronto (1984)

Sih, G.C., Michopoulos, J., Chou, S.C.: Hygrothermoelasticity. Kluwer Academic Publishers, New York (1986)

Straughan, B.: Nonlinear stability for thermal convection in a brinkman porous material with viscous dissipation. Transp. Porous Med. **134**, 303–314 (2020)

Zhang, B., Cheng, Z., Zhang, L.: Numerical simulation for coupled heat and moisture transfer in building material. In: 3rd International Conference on Material, Mechanical and Manufacturing Engineering. IC3ME (2015)

Publisher's Note Springer Nature remains neutral with regard to jurisdictional claims in published maps and institutional affiliations.